ISSN: 2688-8645

Experimental Study on the Rheological Mechanical Properties and Creep Mechanism of Red Mudstone in Central Yunnan

Bo Wang, Yushu Ding

School of Environment and Architecture, University of Shanghai for Science and Technology, Shanghai 200093, China

Abstract

To explore the creep characteristics and mechanism of soft rock from a microscopic perspective, this paper investigates the red mudstone from the Shizishan tunnel section in central Yunnan. A stepwise loading approach was employed to investigate the creep characteristics of the rock samples. A viscous model was established in the 3D particle flow code (PFC), and the discrete element method (DEM) was employed to simulate static fatigue failure of the rock based on experimental data, thereby studying its microscopic creep mechanism. The results show that: (1) Under low stress conditions, the rock samples primarily exhibit decelerating creep, where creep deformation accounts for up to 85% of the total deformation. Under high stress conditions, the rock samples experience the entire creep process, transitioning from decelerating creep, to steady-state creep, and finally to accelerated creep failure, with creep deformation accounting for up to 87% of the total deformation; (2) Shear stress levels significantly affect the creep deformation of rock samples, with a positive correlation between shear stress levels and the time required for decelerating creep to reach a stable state. The proportion of creep deformation in total deformation increases correspondingly; (3) As lateral stress levels increase, the creep strain rate gradually rises. If the stress exceeds the threshold, irreversible stress damage occurs, shortening the creep time; (4) By inserting measurement circles to monitor the coordination number during the loading process, the relationship between porosity and shear mechanism can be determined. The model's overall fit is high, and the behavior of the 3D model during stepwise loading is essentially consistent with that under single-step loading, validating the reliability of the experiment.

Keywords

Rock Creep; 3D Particle Flow Code (PFC); Stress Corrosion Model; Crack Propagation.

1. Introduction

Yunnan Province is characterized by a mountainous plateau topography, with widespread sedimentary rock formations. Among them, mudstone formations exhibit significant rheological properties and often appear in engineering projects as adverse geological structures. Even slight mismanagement can lead to collapse, instability, or large deformations. With the advancement of water diversion projects in Yunnan, the need for earthquake resistance and disaster prevention has driven research into the strength, deformation characteristics, and failure mechanisms of rock masses, which form the foundation for stability analysis of rock formations[1]. Therefore, the red bed soft rock in central Yunnan presents a significant engineering geological problem in the Yunnan Central Water Diversion Project. It is prone to large deformation due to tunnel extrusion, affecting construction and operational safety, necessitating an in-depth study of its rheological mechanical properties and creep mechanism to ensure project safety.

ISSN: 2688-8645

Direct shear tests can effectively simulate the stress conditions and crack propagation along the shear plane of rock masses under different tangential stress conditions. Over the years, scholars have made significant achievements in studying the rheological mechanical properties of rocks, focusing on structural plane shear, uniaxial, biaxial, and triaxial compression load conditions[2]. Yu Qihua[3] proposed a unified rheological model system that integrates the advantages of previous rheological models and supplements the accelerated creep model. Xu Wenlong[4], through his study of Jurassic limestone in southern France, confirmed the existence of the shear plane "p" in brittle shear zones of rocks. Xu Hongfa[5] discussed the time effect of soft rock strength and elastic modulus through uniaxial compression creep tests, analyzing the time effect of rock damage, and proposed the concept of long-term elastic modulus and long-term damage variables. Yang and Daemen[6] studied the influence of temperature on the creep characteristics of rock materials by heating tuff to 204°C and conducting creep experiments, finding that creep deformation increased with temperature under constant load stress, eventually leading to failure. Wang Yao and Wei Jinbing[7] conducted a discrete element analysis of coarse-grained soil creep considering particle breakage based on stress corrosion theory, which can serve as a foundation for further study of creep mechanisms in coarse-grained soil. Song Fei and Zhao Fashuo[8] derived the calculation formula for viscous strain in viscoelastic-plastic damage rheological models in finite element analysis and analyzed the finite element solution process using the initial strain method. Zhang Zelin and Wu Shuren[9] conducted triaxial creep tests on mudstone under different loading methods and moisture contents, observing that mudstone creep deformation increased slowly with stress levels and time, eventually stabilizing at a certain value. Zhao Yanlin[10], based on the lack of classification studies on rock creep strain, proposed a method for separating viscoelastic-plastic strain in rocks through creep experiments and data processing techniques. Huang Jiuyang[11] introduced seven irregular serrated joint profiles to represent the geometric shapes of natural joints and performed direct shear tests on joint specimens under constant normal stress using PFC. The maximum stress value before the shear stress peak was introduced to quantify the contribution of local protrusions to shear stress. Hu Shixing and Jin Xiaoguang[12], using large-scale indoor triaxial tests and the PFC3D/FLAC3D coupling analysis method, established a flexible servo triaxial loading model simulating the shape of partial block stones, where the contact force chain gradually concentrated in areas with more block stones, and axial force was mainly provided by contact between the stones. Meng Xingyu[13], combining indoor true triaxial tests, used the PFC3D discrete element program to numerically calculate the deformation and failure process of rocks under true triaxial stress, revealing the microscopic damage mechanism of rocks under true triaxial conditions.

In recent years, numerical analysis methods have become important tools for analyzing the rheological properties of rocks. Lockner and Madden[14] used the finite difference method to simulate creep deformation of brittle rocks based on renormalization group theory. Xu tao[15] employed finite element methods to study the microscopic creep damage instability mechanism of brittle rocks, considering material heterogeneity and mechanical property degradation. Chen and Konietzky[16] used the block discrete element software to simulate creep instability of brittle rocks based on subcritical crack propagation theory. Tran [17] proposed the rock-ageing model to simulate the creep behavior of dam bodies in stability studies, and Wang yunjia [18] developed the bond-ageing model in the Particle Flow Code (PFC) to simulate creep based on the rock-ageing theory. Potyondy[19], based on stress corrosion theory, established a parallel bond stress corrosion model in the two-dimensional particle flow code PFC2D, and some scholars[20-21] have applied PFC2D to simulate rock creep instability using the discrete element method.

Based on the above dynamic analysis, although scholars have conducted extensive research on the creep of various rocks, further study on the creep characteristics of red mudstone in central

ISSN: 2688-8645

Yunnan is still needed due to its unique geological conditions. The differences in microstructure and approximation between two-dimensional and three-dimensional models are evident. Conducting three-dimensional numerical simulations of creep damage in red mudstone will provide important insights into understanding the microscopic instability processes and mechanisms of mudstone creep in engineering applications.

In this paper, we focus on the red mudstone in the Shizishan tunnel section of the "Yunnan Central Water Diversion Project" and conduct shear tests under different shear stress levels using the stepwise loading method to analyze its creep characteristics. Based on experimental data, we analyze the rock's creep strength using the particle flow software PFC3D and investigate the crack propagation mechanism under different shear forces, providing insights into the correlation between shear mechanical behavior and relevant parameters for the "Yunnan Central Water Diversion Project.

2. Shear Creep Test

The International Society for Rock Mechanics (ISRM) points out that large-scale deformation and instability caused by rock mass extrusion around excavation faces in tunnels and other underground spaces are often due to creep deformation induced by shear strain. Therefore, this study focuses on the shear creep characteristics of the red mudstone in central Yunnan.

2.1. Rock Mechanics Sample

This study is based on the "Central Yunnan Water Diversion" project, where indoor shear creep tests were conducted on red mudstone samples taken from the Haidong tunnel section. These tests aim to investigate the creep characteristics of the red mudstone in central Yunnan and provide reference data for engineering design. First, the rock samples were prepared in accordance with rock mechanics test standards and requirements. The samples were shaped into standard cubic specimens of 100mm × 100mm × 100mm, following the "Standards for Testing Methods of Engineering Rock Masses."

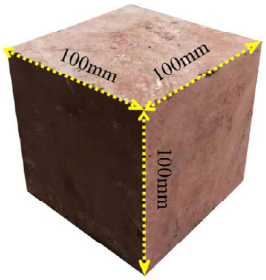

Figure 1. Mudstone samples of the red formation in middle Yunnan

2.2. Test Equipment

The equipment used for this experiment is the CSS-1950 biaxial rheological testing apparatus from the Geotechnical Rheology Laboratory at Tongji University. The apparatus consists of three main components: the main machine, measurement instruments, and a control cabinet The testing machine has a horizontal loading capacity of 300 kN and a normal loading capacity of 500 kN. The measurement instruments consist of both lateral and vertical displacement sensors, which are grating displacement sensors used to measure the horizontal and vertical displacements during the rock shear creep process with an accuracy of up to 0.001 mm. The control cabinet is connected to the main machine to control the application of tangential and normal loads and to transmit deformation data back to the computer, enabling data analysis and processing to meet the requirements of this experiment.

ISSN: 2688-8645

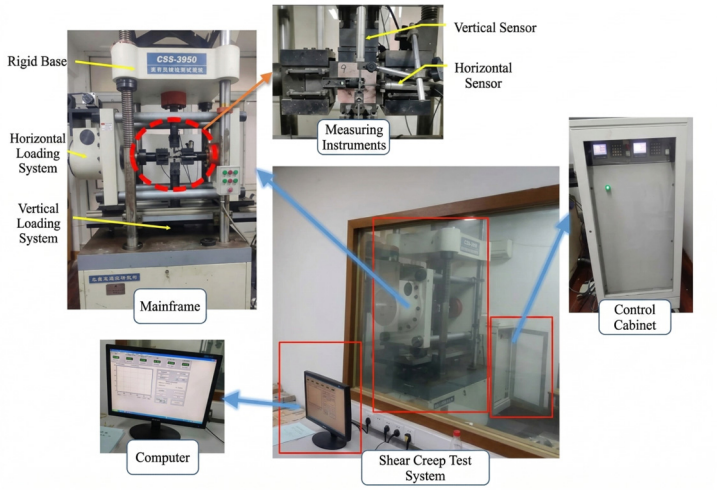

Figure 2. CSS-1950 shear creep meter

3. Experimental Plan

3.1. Test Scheme

Before conducting the shear creep test, a quick shear test was performed on the rock samples to obtain the shear strength values under different normal stress conditions. This also allowed for the calculation of the rock's cohesion (c) and internal friction angle (phi). The quick shear test was carried out in accordance with the "Standards for Testing Methods of Engineering Rock Masses" and the "Rock Testing Code for Hydraulic and Hydropower Engineering." The data obtained from the quick shear test on the red mudstone in central Yunnan are presented in the table.

Using linear least squares fitting, the relationship curve between normal stress and peak shear stress was plotted, as shown in Figure 3. It is evident that there is a clear linear relationship between the peak shear stress and normal stress of the red mudstone in central Yunnan. The fitting equation is (tao= 0.805sigma + 0.333), with a goodness of fit of 0.996. From this, the internal friction angle (phi) is calculated to be 38.83°, and the cohesion(c) is 0.333 MPa.

Table 1. Results of quick shear test of mudstone

argument	Sample numbering				
	J1	J2	J3	J4	J5
Normal stress /MPa	0.2	0.4	0.6	0.8	1.0
Shearing stress /MPa	0.481	0.671	0.818	1.002	1.142

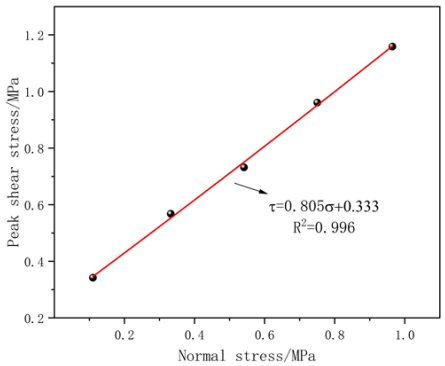

Figure 3. Normal stress and shear stress relationship curve

ISSN: 2688-8645

3.2. Experimental Procedure

1)Place the prepared rock sample on the test platform and adjust its position so that its centerline aligns with the vertical loading axis of the apparatus. Then place spacers and a rigid roller on top of the rock sample to ensure uniform loading and to minimize friction between the vertical loading head and the rock sample during the application of normal stress.

2) Attach lateral and vertical displacement sensors to the sides of the rock sample to record the sample's displacement during the test.

3) First, apply the normal stress. Once the vertical deformation stabilizes, progressively apply shear loads.

4) For each level of applied shear load, the computer automatically collects shear displacement data. Once the creep time for that load level is reached, proceed to the next shear load level. The test continues until the final load level is applied or until the sample undergoes creep failure, marking the end of the experiment.

Throughout the experiment, the environmental temperature and humidity should be kept as constant as possible, with temperature fluctuations not exceeding 1°C.

4. Analysis of Laboratory Test Results

After sorting out the shear creep test, the creep curve of the rock under graded loading conditions is shown in the figure:

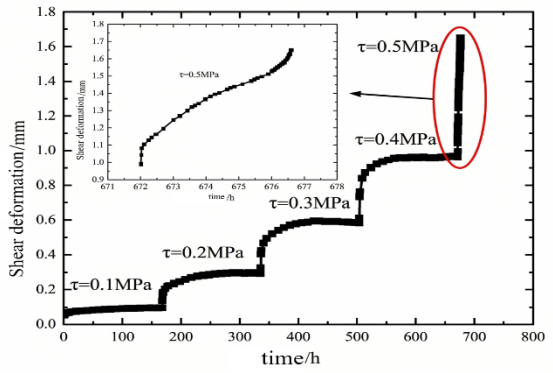

Figure 4. Diagram of fractional shear creep strain

Due to the stepwise loading method used, the resulting curves exhibit a stepped creep pattern. To facilitate the study of the creep characteristics of red mudstone in central Yunnan, the Chen's loading method will be applied to process the test data. According to this method, the displacement-time curve for the first load level remains unchanged, and for the second load level, the creep increment corresponding to the duration of the second load is superimposed on the first load's curve. This approach yields the creep curve under the influence of the second load level alone.

In summary, when the shear stress level is high, the red mudstone in central Yunnan undergoes the complete process of decelerating creep, steady-state creep, and accelerated creep. Among these, steady-state creep constitutes the largest portion of the three stages, indicating that the red mudstone exhibits significant time-dependent effects.

When the shear stress level is low (100 kPa to 400 kPa, as shown in Figure 5), after the rock sample undergoes instantaneous shear deformation, the shear deformation continues to increase with loading time, but the rate of increase gradually decreases until it stabilizes at a constant value. The entire deformation process exhibits a clear trend of decelerating creep. At a shear stress of 100 kPa, after 40 hours of decelerating creep, the creep strain stabilizes at 8.95

ISSN: 2688-8645

× 10^{-4}, accounting for approximately 47% of the total strain. At a shear stress of 200 kPa, after 90 hours of decelerating creep, the creep strain stabilizes at 40.91 × 10^{-4}, representing about 69% of the total strain. At a shear stress of 300 kPa, the decelerating creep lasts for 110 hours, and the creep strain reaches 92.73 × 10^{-4}, approximately 80% of the total strain. At a shear stress of 400 kPa, after 120 hours of decelerating creep, the creep strain stabilizes at 163.72 × 10^{-4}, which is about 85% of the total strain.

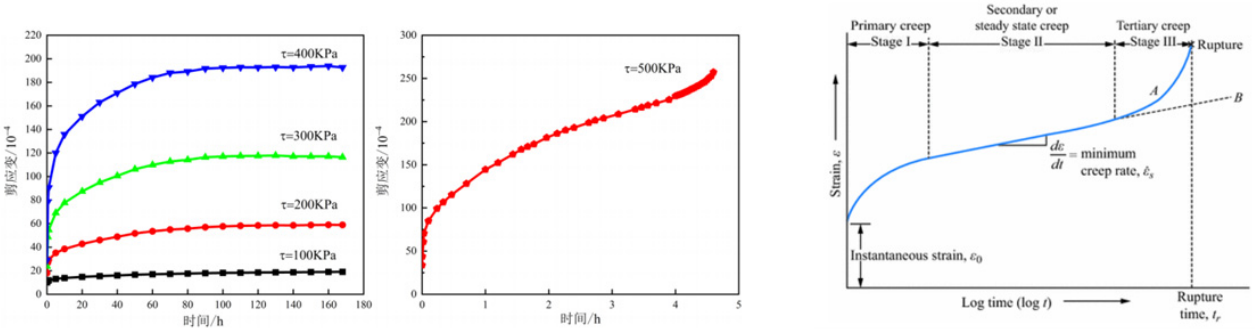

Figure 5. Creep curve and creep mechanism of rock samples under different shear stress levels

This indicates that the red mudstone in central Yunnan exhibits strong time-dependent deformation behavior. Even in the case of decelerating creep, the creep strain can account for a high proportion of the total deformation, reaching up to 85%. Compared to hard rocks and ordinary soft rocks, the time-dependent deformation of red mudstone is more pronounced. Additionally, shear stress levels have a significant impact on the creep of rock samples: the higher the shear stress, the longer it takes for decelerating creep to reach a stable state, and the higher the proportion of creep deformation in the total deformation. This suggests that the higher the shear stress, the more prone the red mudstone is to creep.

5. Rock Creep Particle Flow Model

5.1. Parallel-Bond Stress Corrosion Model

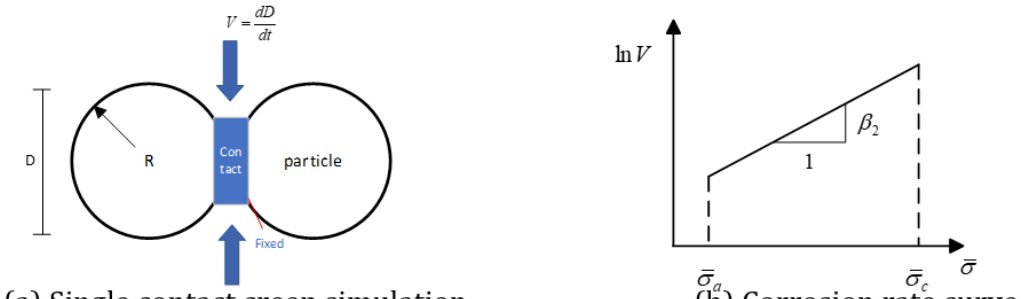

(a) Single contact creep simulation (b) Corrosion rate curve

Figure 6. PSC model

In the native substratum, rocks subjected to constant confining pressure loads over many years experience crack propagation. When these cracks expand to a subcritical state, stress corrosion occurs, and the mechanical parameters that provide resistance gradually weaken over time. In the particle flow model, this progressive expansion of microcracks, caused by stress corrosion over time, is modeled through the dense packing of particles of different sizes, with the mechanical interactions between particles simulated using the discrete element method. This captures the mechanism by which microcracks nucleate, grow, and interact under stress damage, reflecting the subcritical crack propagation in the rock at the macroscopic level.

ISSN: 2688-8645

The mechanical properties between particles are represented using the Parallel-bond Stress Corrosion (Psc) model, as shown in Figure 6(a). In this model, stress corrosion is introduced into the particle bonding process, simulating the static fatigue failure of the rock. The Psc model assumes that stress corrosion occurs at the parallel bond contacts between particles. The bonding force between contact pairs gradually decreases based on the relationship between shear stress and crack propagation rate. During this phase, the bond strength transitions from compressive stress to tensile stress and continues to endure tension until it exceeds the tensile stress threshold, at which point microcracks begin to form progressively.

psc crack growth rate model formula:

$$\frac{d\bar{D}}{dt}=\begin{cases}0, & \bar{\sigma}<\bar{\sigma}_a\\ -\beta_1 e\beta_2^{\left(\frac{\bar{\sigma}}{\bar{\sigma}_c}\right)}, & \bar{\sigma}_a<\bar{\sigma}<\bar{\sigma}_c\\ -\infty, & \bar{\sigma}>\bar{\sigma}_c\end{cases} \tag{1}$$

In the formula: $\bar{D}$ is the average diameter of parallel bond bonding; t is time; $\bar{\sigma}$ is the maximum tensile stress of parallel bond bonding between particles; $\bar{\sigma}_a$ is the threshold of intergranular stress corrosion; $\bar{\sigma}_c$ is the threshold of intergranular tensile strength; β_1、β_2 is material coefficient;

$$\bar{E}_k=\frac{1}{2}\left(\frac{\bar{F}_n^{\,2}}{\bar{k}_n\bar{A}}+\frac{\left\|\bar{F}_s\right\|^2}{\bar{k}_s\bar{A}}+\frac{\bar{M}_t^{\,2}}{\bar{k}_s\bar{J}}+\frac{\left\|\bar{M}_b\right\|^2}{\bar{k}_n\bar{I}}\right) \tag{2}$$

In the formula: $\bar{E}_k$ is Strain energy; $\bar{F}_n$、$\bar{F}_s$ are normal and tangential forces respectively; $\bar{k}_n$, $\bar{k}_s$ are normal and tangential strength respectively; $\bar{M}_t$、$\bar{M}_b$ are tangential and normal moments respectively; $\bar{I}$, $\bar{J}$ are the moment of inertia at the contact and the polar moment of inertia; A is the contact area of the parallel bond（The contact area in PFC2D is $2\bar{R}t$, $t=1$; The contact area in PFC3D $\pi\bar{R}^2$）

5.2. Transient Mesoscopic Parameter Calibration

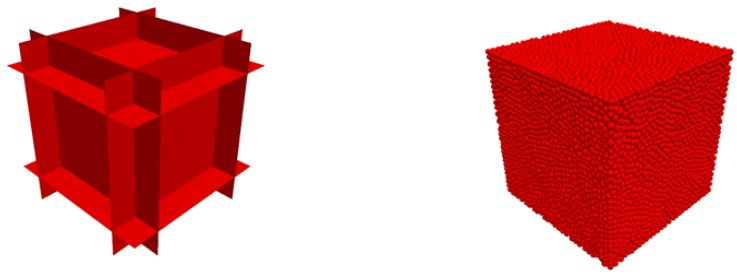

Figure 7. PFC shear creep model

The transient microscopic parameter calibration of the model is based on the macroscopic mechanical parameters from laboratory shear tests on rocks, such as the shear strength values under different normal stress conditions, cohesion (c), and internal friction angle (phi) from quick shear tests. By establishing a PFC discrete element model and adjusting the bond strength between particles to generate damage-induced microcracks, a comparison is made between the macroscopic mechanical parameters of the model and the shear mechanical parameters obtained from laboratory tests as a reference.

ISSN: 2688-8645

In this study, the shear creep test of the red mudstone in central Yunnan was conducted at the Geotechnical Rheology Laboratory of Tongji University using cubic rock samples measuring 100mm × 100mm × 100mm for direct shear tests. The internal friction angle (phi) was determined to be 38.83°, and the cohesion (c) was 0.333 MPa.

In PFC, the interaction between particles is modeled using parallel bond contacts, which simulate the contact between soil particles. The microscopic parameters of the particles are shown in Table 1. These parameters are crucial for accurately replicating the mechanical behavior of soil particles in the simulation, ensuring that the particle interactions reflect the real-world stress and strain conditions observed in the shear tests. The table includes parameters such as particle stiffness, bond strength, and friction coefficients, which are key to modeling the deformation and failure mechanisms in the material.

Table 2. Model parameters table

Parameter/unit	Numerical value
Minimum radius of particle /mm	2.0
Maximum radius of particle /mm	2.5
Particle radius ratio	1.25
Elastic modulus of particles /GPa	0.1
Particle stiffness ratio	0.2
Particle friction coefficient	0.5
Wall friction coefficient	0
Average bond contact tensile strength /MPa	20
Average tangential strength of adhesive contact /MPa	32

Based on the microscopic parameters, a PFC particle flow model is established. The model is first subjected to a normal stress of 200 kPa, and a quick shear test is performed. The stress-strain curve is shown in Figure 8. As the shear stress is applied tangentially, the stress gradually transfers from the edge particles of the rock to the center through the inter-particle interaction forces. This stress transfer mechanism is crucial in simulating the progressive shear deformation of the rock, where the particle bonds at the edges begin to break, and the internal stress is redistributed, leading to crack propagation and eventual failure as observed in the stress-strain behavior.

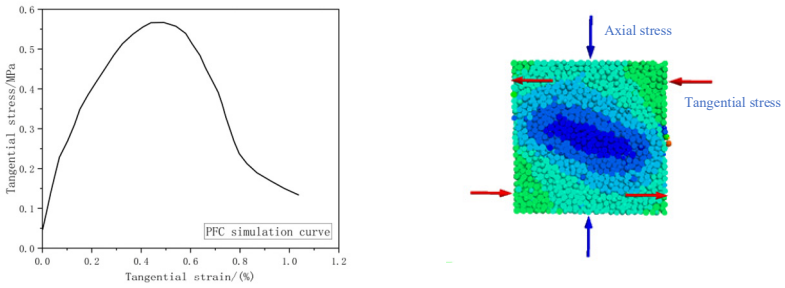

(a) stress-strain curve (b) Sample model diagram of direct shear numerical test

Figure 8. Simulation of shear failure

ISSN: 2688-8645

5.3. Multi-level Parameter Calibration

The shear strength of rock is its ultimate resistance to shear failure and is typically measured using direct shear tests. In this study, to calibrate the rock mass properties, the PFC software was utilized to establish a discrete element model. Numerical convergence calculations were repeatedly performed to replicate the macroscopic properties of the rock mass. This approach calibrates a set of internal particle interaction parameters that match the results of the laboratory tests, laying a solid foundation for subsequent analysis of creep characteristics.

The shear creep test was conducted using a stepwise loading method. After the quick shear test, the shear peak stress of the rock sample under a normal stress of 200 kPa was determined to be 563 kPa. The stepwise loading method was applied again for the shear creep test, using the same normal stress. The 90% peak shear stress was divided into five loading stages. Each stage of the shear creep test lasted for 168 hours until the rock sample was completely destroyed. The details of the shear test for each stage are provided in Table 3.

This method ensures a thorough examination of the creep behavior under progressively increasing shear loads, allowing for the precise identification of the rock's creep limits and deformation characteristics at each stress level.

Table 3. Loading parameters

Normal load σ/kPa	Shear load τ/kPa				
200	Level1	Level2	Level3	Level4	Level 5
	100	200	300	400	500

The following is the procedure for conducting a shear creep test using the calibrated model in PFC:

1) Apply Constraints: To achieve rigid constraints in the PFC software, a rigid wall structure is established. A wall in PFC is composed of a series of facets and is generally a massless rigid structure in 3D, with no force transmission between the facets. After creating the wall, a velocity of zero is assigned to simulate the base of the laboratory experiment.

2) Particle Generation: The particle characteristics include particle gradation, porosity, damping coefficient, density, stiffness ratio, and modulus. The target porosity for the sample is set to 0.8, ensuring minimal particle overlap during packing. Using the calibrated parameters, exact data is obtained, and the particle interactions are restored through pre-consolidation.

3) Generate Bonds: After pre-consolidation and stabilization of the sample, bonds are generated between particles in a single step. The bond radius is set to 1mm, simulating the cementation process in mudstone. The bonded sample is then unloaded to an isotropic compression state.

4) Loading: Shear loads are applied incrementally to the sides of the rock mass. After each load level reaches the creep duration, the program proceeds to the next level of shear loading. Each load level differs by 100 kPa, continuing until a maximum of 500 kPa is reached or the rock mass undergoes irreversible creep failure, at which point the experiment ends.

Note: Throughout the experiment, environmental conditions such as temperature and humidity are kept constant.

6. Analysis of Deformation and Failure Characteristics

6.1. Analysis of Rock Creep Characteristics under Graded Loading Conditions

Based on the comparison with laboratory data, the simulated creep curves of the rock mass under stepwise loading conditions are as follows:

ISSN: 2688-8645

These curves reflect the deformation behavior of the rock mass at different shear stress levels, showing the transition from initial decelerating creep to steady-state creep and, eventually, accelerated creep leading to failure at higher stress levels. The accuracy of the simulated curves, when compared with the experimental data, validates the effectiveness of the PFC model and the calibrated parameters, providing insights into the rheological behavior of the red mudstone under these conditions.

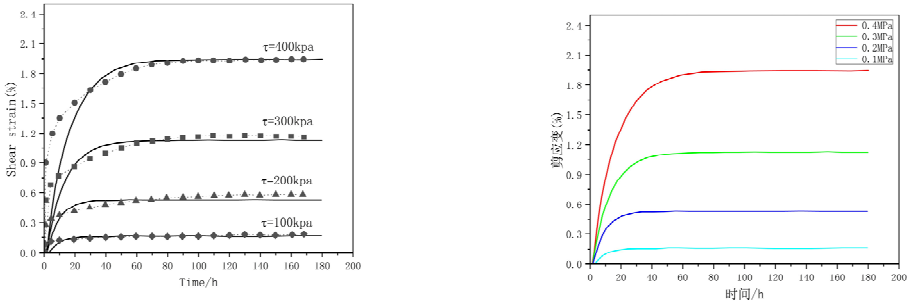

Figure 9. Creep curves of rock under different shear stress levels

In laboratory experiments, due to the inherent variability in the mechanical properties of rock samples, experimental data can sometimes show significant dispersion. Therefore, stepwise loading tests are employed to reduce data variability and shorten testing times. In PFC3D, stepwise loading is implemented by controlling the displacement of the walls to achieve incremental loading of the rock model. The loading process is divided into four levels, starting from 20% of the stress level and increasing up to 80% of the stress level (20%, 40%, 60%, and 80%), with each stage increasing the shear stress by 100 kPa. Each loading stage is simulated for 170 hours. Once the load reaches 90% of the stress level, the stress is maintained constant until the model fails.

Table 4. Shear plane crack expansion and evolution of direct shear numerical test samples with shear strain

Shear strain /%					
0.5	1	1.5	2	2.5	3
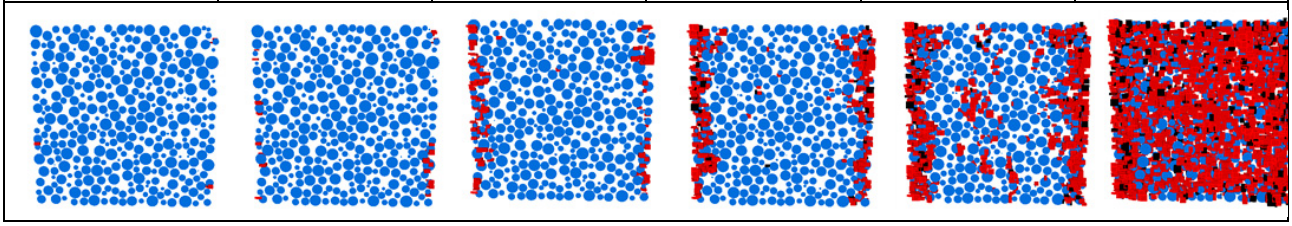					

To further analyze the microcrack propagation and evolution process on the shear plane, slices were observed at different stages of shear strain. The results are shown in Table 2. In the red mudstone from central Yunnan studied in this paper, cracks increase with rising shear stress, starting at the edges and eventually leading to full fragmentation.

- At a shear strain of 0.5%, during the early quasi-static loading phase, no cracks were observed.
- At a shear strain of 1.0%, initial cracks began to appear at the edges of the sample.
- At a shear strain of 1.5%, a large number of cracks formed at the edges, though the core area remained intact, indicating that the rock was transitioning from the linear to the plastic phase.

ISSN: 2688-8645

- At a shear strain of 2.0%, the edges were fully fractured, and cracks began to appear in the core region, marking the stress decay phase with numerous tensile failure cracks.

Finally, in the residual strength phase (shear strain of 2.5% to 3.0%), as shown in Figure 8, both compressive and tensile failure were widely distributed across the entire shear plane, including both ends and the middle, consistent with the stress distribution pattern observed.

According to the data in Figure 9, it can be seen that the rock mass failure velocity simulated by pfc shows a slow increasing trend, because the loading rate is different from the curve in the laboratory. In the process of 100-400kPa, the simulated duration of the rock remains unchanged, and the creep strain rates of the steady creep stage are 0.16%, 0.52%, 1.12% and 1.94%, respectively, indicating that the shear stress has a great influence on the stress corrosion strain rate. Every 100kPa increase, the strain itself increases by at least 70%.

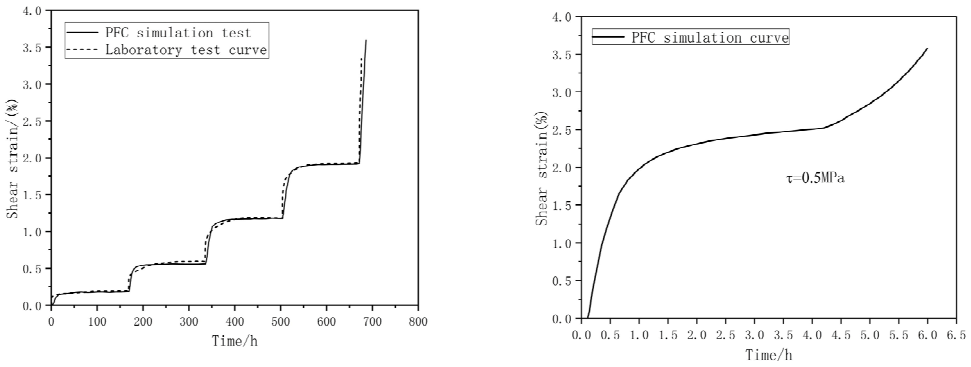

Figure 10. Creep curve of rock mass under graded loading

Figure 10 shows the data plot for the stepwise loading of the sample after parameter calibration and the creep data under a shear force of 500 kPa. The dashed line represents the experimental stress-strain step plot, while the solid line represents the step plot obtained from the model simulation. It can be observed that the force loading in the PFC software is not as sensitive as in the experiment, but the overall trend remains consistent.

Comparing the particle flow model with the experimental data reveals little structural difference, which indirectly confirms the original elasto-plastic contact structure of the red mudstone in central Yunnan. When a larger shear stress is suddenly applied after the model reaches 400 kPa, the creep enters an accelerated phase. The failure trend at this stage is depicted in the figure, indicating a rapid progression towards instability and eventual fracture, consistent with the experimental observations.

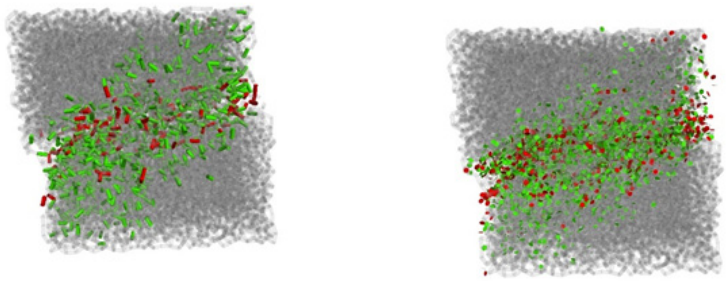

Figure 11. Map of microcrack distribution

Under the stepwise loading conditions, the lateral strain of the rock mass exhibited a significant creep response, both during the initial shear deformation and in the stable state. When the

ISSN: 2688-8645

shear stress level is low, after the rock mass undergoes shear deformation, there is a certain amount of displacement response due to creep. The shear deformation gradually stabilizes over time, showing a clear trend of decelerating creep. At lower shear stress levels, the deformation of the rock mass is primarily elastic, and the dynamic response is quicker. As the stress continues to increase, creep becomes more apparent, and the rock enters a phase of slow strain growth. Eventually, at the same stress level, the lateral creep stress weakens and stabilizes into a steady deformation.

From a microscopic particle contact perspective, as the stress is gradually applied, when the stress reaches the fracture threshold of the cementing material at a low level, microcracks begin to propagate. This is predominantly characterized by tensile failure (green disks represent tensile failure, while red disks indicate compressive failure). The initiation and expansion of these microcracks correspond to the stress-induced damage, further explaining the observed creep behavior under increasing shear stress.

6.2. Analysis of Deformation and Force Chain Evolution Characteristics of Two-Dimensional Creep Simulation

Figure 16 shows the particle motion trajectories and velocity vector diagram of the mudstone sample under a vertical confining pressure of 200 kPa and a lateral shear stress of 400 kPa. From the figure, it is evident that the shear forces in two lateral directions cause the transmission of force between the particles within the sample. The particle motion vectors in the central region exhibit a noticeable bifurcation displacement, splitting the originally horizontal shear motion into upward and downward movements.

The blue regions represent the areas with the slowest displacement, where there is minimal relative movement between particles. The green areas, particularly at the ends, form a rectangular shape with a triangular void, experiencing primarily horizontal displacement, indicating that this region remains largely undisturbed and can be considered an elastic zone.

In the central region, particle motion is predominantly influenced by tangential shear forces. As particles get closer to the middle of the sample, their motion vectors increasingly deviate toward the vertical direction. This pattern shows that in the shear zone, particle displacement vectors shift with increasing strain, initially exhibiting compaction and later showing deflection. These observations align with the direction of microcrack propagation in the 3D simulation, confirming the consistency between the experimental results and the modeled microstructural behavior.

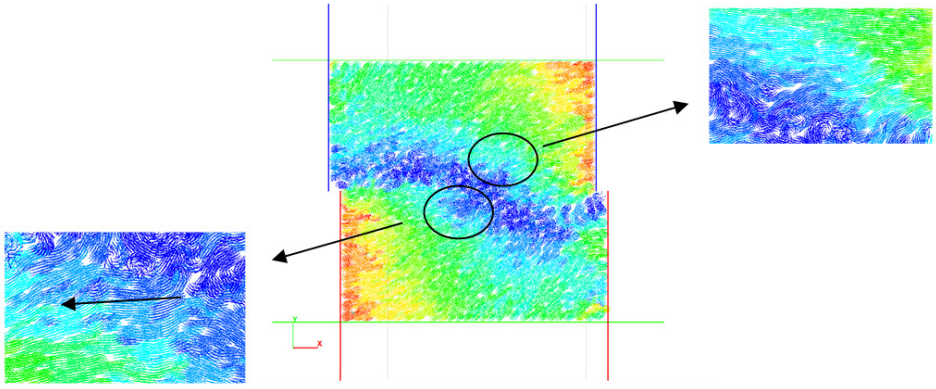

Figure 12. Displacement direction of particles

In the blue region, it behaves more like a "latch" that firmly holds the elastic region together, redistributing the shear force that should be acting across the sample to the internal particles in the vertical direction.

ISSN: 2688-8645

To further analyze the development of the shear band within the sample during the test, three measurement circles were established along different locations on the x-axis of the rock sample. These circles were used to measure the porosity of particles in real time at various positions. As shown in Figure 10, at the initial loading stage, particles in all regions of the sample exhibited disordered movement, with no clear connections and relatively low speeds, reflecting the characteristics of initial compression. This stage marks the rearrangement and compaction of particles before the more localized shear zones start to form, indicating the beginning of internal structure changes within the sample.

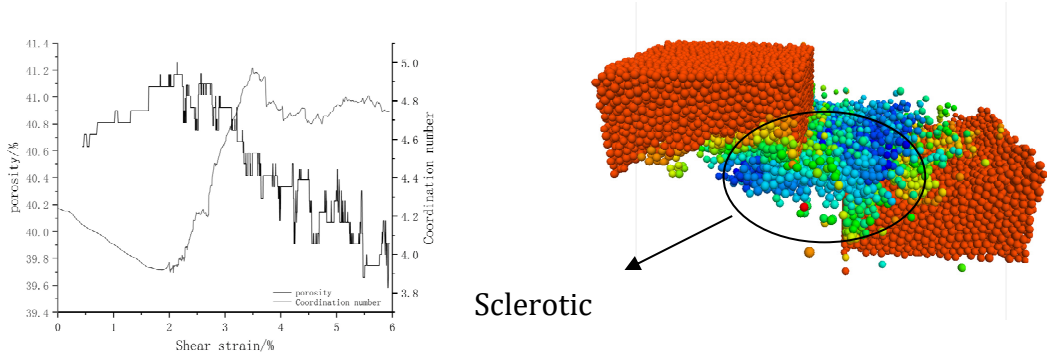

Figure 13. Pore ratio and coordination figure of rock samples under 400kPa confining pressure

The coordination number, which represents the number of contacts between particles, is an important indicator of how tightly packed a granular system is and provides a basis for evaluating the number of contacts between particles. When a rock is compressed by external forces, if the number of particles and the weight remain unchanged, a reduction in volume indicates a decrease in porosity. As air is compressed and escapes, the contact between soil particles becomes more solid, significantly contributing to the rock's macroscopic load-bearing capacity. The coordination number is the parameter that reflects this phenomenon. Conversely, when particles become loose, it indicates a weakened ability of the rock to transmit supporting forces.

Figure 13 presents the trends of coordination number and porosity under a shear stress of 400 kPa. In the figure, the left y-axis represents porosity, and the right y-axis represents the coordination number. From the graph, it can be observed that during the initial application of shear stress, the coordination number of the central particles increases, while the porosity decreases, indicating that the particles are in a compressed state, which corresponds to the hardened part of the sample.

Once the tangential strain exceeds 2%, the porosity begins to increase, and the coordination number decreases. This stage reflects the onset of tangential deformation, with significant dilatancy effects becoming apparent. When the tangential strain surpasses 3.5%, the porosity gradually stabilizes as the rock fractures, indicating that the bonding material between the particles in the fracture zone has broken down. This results in macroscopic shear failure of the rock, leading to the formation of a fracture.

7. Conclusion

Based on indoor shear experiments and using the PFC3D analytical method, a servo shear loading model was established to replicate the shape of mudstone. Through numerical analysis, the sensitivity of rock to creep corrosion parameters, deformation and failure characteristics, and the development of shear surfaces and contact force chains were examined. The following conclusions were drawn:

ISSN: 2688-8645

1. The rock samples exhibit two different creep behaviors depending on the applied shear stress. At low stress levels, below the long-term strength of the sample, only decelerating creep occurs. At higher stress levels, exceeding the long-term strength, the rock progresses from decelerating creep to steady-state creep and eventually accelerates into complete failure.

2. In stress corrosion analysis, parameters such as sigma A, beta1, and beta2 have a nonlinear impact on creep deformation, as shown through sensitivity tests. Thus, at different shear stress levels, the stabilized post-creep strain increases progressively after the deceleration phase.

3. During rock failure, under shear stress, the Discrete Fracture Network (DFN) model was introduced to monitor the spatiotemporal evolution of microcracks during creep. The interactions between particles reflected in the microcracks showed that tensile failure was predominant, with shear cracks secondary, forming macroscopic fracture zones under shear conditions.

4. When introducing the discrete element method in PFC3D along with the PSC corrosion model, the failure shear band of the rock sample appeared in an elliptical distribution, with an inverted triangular shape in space. The internal part remained elastic, and the so-called long-term strength relied on this elastic deformation. If microcracks propagated in this region, it would inevitably lead to accelerated creep development.

5. Under a 400 kPa confining pressure, during the loading process, when the tangential strain was less than 1.8%, the coordination number increased with strain while porosity decreased, indicating a compacted state. When the tangential strain exceeded 1.8%, the coordination number decreased, and the porosity increased, as the sample began to fracture and a continuous shear band formed, exhibiting dilatancy characteristics.

6. Comparing the model with experimental results, the simulated results under the calibrated PFC parameters align well with experimental data. This demonstrates that modeling in PFC can effectively capture the creep behavior of soft red mudstone in central Yunnan under shear failure, making it highly applicable for future simulations of Yunnan rock layers.

References

[1] Y.J. Wang. Causes and Treatments of Cracks in Turbine Runners of Yantan and Lijiaxia Hydropower Stations [J]. Water Power, 1999, 05: 43–45.

[2] S.J. Shao, F.F. Zhou, J,Y. Llong. Structural properties of loess and its quantitative parameter [J]. Chinese Journal of Geotechnical Engineering,2004, 4 : 531-536.

[3] Q.H. Yu. Rheological failure process of rock and finite element analysis [J]. Journal of Hydraulic Engineering , 1985, 1: 65-66.

[4] W.L. Xu. Study on micro-fractures in brittle shear zones of rocks [J]. Journal of Southwest Jiaotong University,1995, 30(3): 245-251.

[5] H.F. Xu. Study on the time effect of soft rock strength and elastic modulus [J]. Chinese Journal of Rock Mechanics and Engineering, 1997, 16(3): 246—251.

[6] C.H. Yang, J.K. Daemen. Temperature effects on creep of tuff and its time-dependent damage analysis[J]. International Journal of Rock Mechanics and Mining Sciences1997,34 (3/4): 345-357.

[7] Y. Wang, J.B. Wei, R.J. Wen, et al. Influencing Factors Analysis of Stress Corrosion Creep for Coarse-grained Soils Based on Discrete Element Method [J]. Journal of Water Resources and Architectural Engineering, 2020, 18(3): 87-92.

[8] F Song, F.S. Zhao, Y.L. Li. Damage rheological constitutive model for numerical simulation to gypsum breccias [J]. Advances in Science and Technology of Water Resources, 2008, (1): 12-15.

[9] Z.L. Zhang, S. R. Wu, T. Wang, et al. Study on shear creep behavior and its model of mudstone in Tianshui, Gansu Province [J]. Chinese Journal of Rock Mechanics and Engineering, 2019, 38(2): 3603-3617.

ISSN: 2688-8645

[10] Y.L. Zhao, J.Z. Tang, C.C. Fu, et al. Rheological test of separation between viscoelastic-plastic strains and creep damage model [J]. Chinese Journal of Rock Mechanics and Engineering, 2016,35 (7): 1297-1308.

[11] J.y. Huan, M.M. He, Z.Q. Zhang, et al. An Investigation on Local Shearing Mechanisms of Irregular Dentate Rock Joints Using the PFC[J]. Geofluids, 2022: 1-20.

[12] S. X. Hu, X. J. Jin, G. D. Sun , et al. Triaxial test and PFC-FLAC coupling simulation study on material parameters and deformation characteristics of soil-rock mixture [J]. Chinese Journal of Rock Mechanics and Engineering, 2021, 40(202): 3344-3356.

[13] X. Y. Meng, Y.L. Lu, L. G. Wang, et al. True triaxial test and mesoscale simulation study of coal-bearing sandstone [J]. Mining Research and Development, 2019, 39(2): 66-69.

[14] Lockner D A, Madden T R. A multiple-crack model of brittle-fracture [J]. Journal of Geophysical Research-Solid Earth, 1991, 96(B12): 19643—19654.

[15] T. Xu, C. H. Tang, J. Zhao, et al. Modelling the time-dependent rheological behaviour of heterogeneous brittle rocks [J]. Geophysical Journal International, 2012,189(3): 1781—1796.

[16] W. Chen, Konietzky Heinz. Simulation of heterogeneity,creep, damage and lifetime for loaded brittle rocks [J].Tectonophysics, 2014, 633: 164—175.

[17] T. H. Tran, R. Vénier, B. Cambou. Discrete modelling of rock-ageing in rockfill dams [J]. Computers and Geotechnics, 2009, 36(1): 264—275.

[18] Y. J. Wang, Z. H. Zhao, S Erxiang. Discrete element modeling of the effect of particle shape on creep behavior of rockfills [J]. International Journal of Environmental, Engineering,2017, 11(9): 803—807.

[19] Potyondy D O. Simulating stress corrosion with a bonded-particle model for rock [J]. International Journal of Rock Mechanics and Mining Sciences, 2007, 44(5):677—691.

[20] N. Liu, C. S. Zhang, W. J. Chu. Simulating time-dependent failure of deep marble with particle flow code [J]. Chinese Journal of Rock Mechanics and Engineering, 2011, 30(10): 1989—1996.

[21] J. S. Sun, M. Chen, Q. H. Jiang, et al. Numerical simulation of mesomechanical characteristics of creep demage evolution for Jingping marble [J]. Rock and Soil Mechanics, 2013, 34(12): 3601—3608.